

Prediction of UHPFRC panels thickness subjected to aircraft engine impact



Duc-Kien Thai^a, Seung-Eock Kim^{b,*}

^a Department of Civil Engineering, Vinh University, 182 Le Duan Street, Vinh City, Nghe An Province, Viet Nam

^b Department of Civil and Environmental Engineering, Sejong University, 98 Kunja-dong, Kwangjin-ku, Seoul 143-747, South Korea

ARTICLE INFO

Article history:

Received 13 November 2015

Received in revised form 5 February 2016

Accepted 14 March 2016

Available online 16 March 2016

Keywords:

Aircraft engine impact

UHPFRC panel

LS-DYNA

Dynamic analysis

Local damage

ABSTRACT

In the practical design of nuclear building structures subjected to an aircraft crash, the structures are required to prevent scabbing and perforation. NEI 07-13 provided the formulas to predict the minimum reinforced concrete (RC) wall thickness to prevent the local damage caused by aircraft engine impact. However, these formulas may not be suitable for predicting the thickness of the ultra-high performance fiber reinforced concrete (UHPFRC) wall. In this study, the local damage of a UHPFRC wall caused by the impact of aircraft engine missile is investigated using a finite element program LS-DYNA. The structural components of the UHPFRC panel, aircraft engine model, and their contacts are fully modeled. The analysis results are verified with the test results. A parametric study with varying panel thickness, fiber type and content, and impact velocity is performed to investigate the local damage of the UHPFRC panel. Based on a comparison with the given formulas, the modified equations of Chang and Degen are proposed to predict the minimum wall thickness to prevent scabbing and perforation in the case in which the UHPFRC structure is used.

© 2016 Published by Elsevier Ltd. This is an open access article under the CC BY-NC-ND license (<http://creativecommons.org/licenses/by-nc-nd/4.0/>).

1. Introduction

UHPFRC structures have been widely used in industry due to its multiple advantages. Literature researches showed that the shear and cracking resistant capacities were the greatest advantages of this structure. Recently, many researchers focused on studying the punching behavior of the UHPFRC panels under impact loading. Riedel et al. [1] performed an experimental series of the UHPFRC panels subjected to the impact of aircraft engines missiles. Their test results showed that in all cases, a significant improvement of punching resistance of UHPFRC panels was observed as compared with that of conventional concrete panels. A series of small-scale of UHPFRC slabs subjected to deformable and non-deformable projectile impacts was also carried out by Sovják et al. [2] and Máca et al. [3]. UHPFRC was verified as having much greater resistance to impact loading compared to traditional FRC.

Various authors have proposed many empirical formulae for local concrete damage prediction as summarized in the work of Adeli and Amin [4]. Accordingly, the penetration depth, scabbing, and perforation thickness of RC panels can be predicted as the function of the impact velocity, concrete strength, reinforcement effect, missile diameter, weight, and nose type. Riera [5] also proposed equations for computing penetration depth and the scabbing and perforation velocities of projectiles impinging normally against plain or RC structures. To study the effect of the projectiles deformation to the local behavior

* Corresponding author.

E-mail address: sekim@sejong.ac.kr (S.-E. Kim).

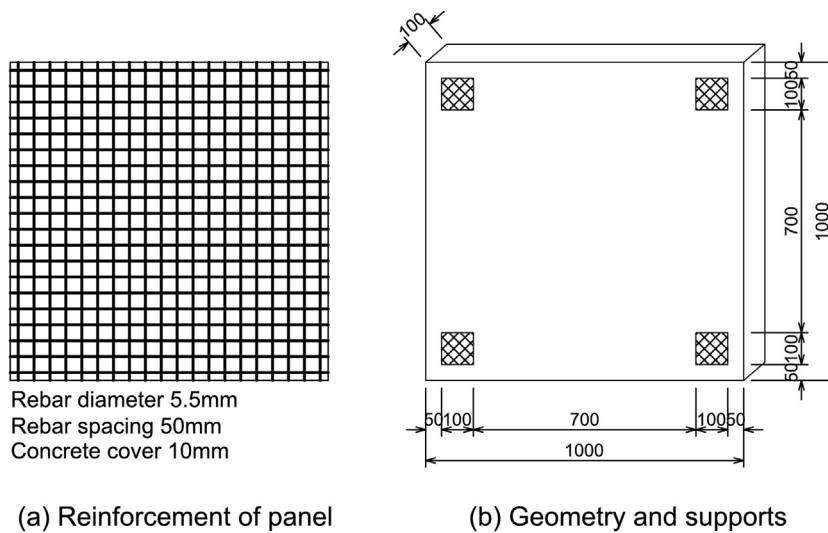


Fig. 1. Geometry of the UHPC panel [1].

of RC panels, Kojima [6] performed a series of missile impact tests of RC slabs with hard-nosed and sort-nosed missiles. In the same way, Sugano et al. [7] introduced reduction factors to quantitatively evaluate the reduction in local damage due to the deformability of engine missiles. Based on Sugano's results, NEI 07-13 [8] provided formulas to predict the minimum RC wall thickness to prevent local damage caused by aircraft engine impacts. The empirical formulas proposed in the literature were based on the experimental results of impact tests of RC panels.

As mentioned above, test results of Riedel et al. [1], Sovják et al. [2], and Máca et al. [3] showed that UHPFRC panels had much greater resistance to impact loading compared to traditional RC panels. Therefore, the above-mentioned empirical formulas may not be suitable for predicting the thickness of the UHPFRC walls.

To address the limitations of the given formulas, this work focused on a numerical analysis of UHPFRC panels subjected to the impact of an aircraft engine model. The analysis results were verified using the test results conducted by Riedel et al. [1]. A parametric study of varying panel thicknesses, fiber types and content, and impact velocities is performed to investigate the local damage of the UHPFRC panels. Based on a comparison with the given empirical formulas, the modified equations of Chang and Degen are proposed to predict the minimum wall thickness to prevent scabbing and perforation in cases in which the UHPFRC structure is used.

2. Analysis model

2.1. FE model for impact simulation

For the purposes of this study, an impact test of UHPFRC panels subjected to an aircraft engine model, carried out by Riedel et al. [1], was adopted. The UHPFRC panels, longitudinal rebars, and aircraft engine were modeled separately and assembled to subsequently develop the full model using LS-PREPOST V4.2. The appropriate constraints and contacts were applied between all contact surfaces. The finite element code, LS-DYNA (version 971s R5.1.1) [9], was used for analysis.

Fig. 1 shows the geometry of the UHPFRC panels with reinforcement and supports. The two-way panel had a total length of $1.0\text{ m} \times 1.0\text{ m}$, a clear span of 0.7 m , and a thickness of 0.1 m . 40 rebars of 5.5 mm diameter with a concrete cover of 10 mm were used as shown in Fig. 1a. The UHPFRC panels were clamped to the support system as shown in Fig. 1b. Fig. 2 shows the FE modeling of the UHPFRC panels. The concrete panel was modeled with a solid element. The Hughes-Liu beam element (type 1) was used to model the longitudinal rebars.

Fig. 3a shows the geometry of the aircraft engine model. The deformable engine model with a scale factor of $1/10$ had a total length of 237 mm and a diameter of 76 mm . The engine model was assembled from three steel sabot rings and two steel cylinders. Fig. 3b shows an FE modeling of the aircraft engine model. The steel sabot rings were modeled with the solid element. The shell element was used to model the steel cylinders.

Table 1 lists the material properties of the concrete, rebar, and aircraft engine model. The concrete had the unconfined compressive strength in the range of $172.1\text{--}186.0\text{ MPa}$. The yield strength of the steel rebar was 447.2 MPa . The failure strain of the steel rebar was 25.0% . The yield strength of the steel aircraft engine model was 335 MPa . The general mesh size was about 10 mm . The total number of elements of the components is shown in Table 2.

The component models were assembled with appropriate constraints and contacts. The longitudinal rebars were embedded in the concrete using the option *CONSTRAINED_LARGRANGE.IN_SOLID. The option *AUTOMATIC_SURFACE_TO_SURFACE was used to model the contact between the aircraft engine model and the panel. The segment set of the aircraft engine model

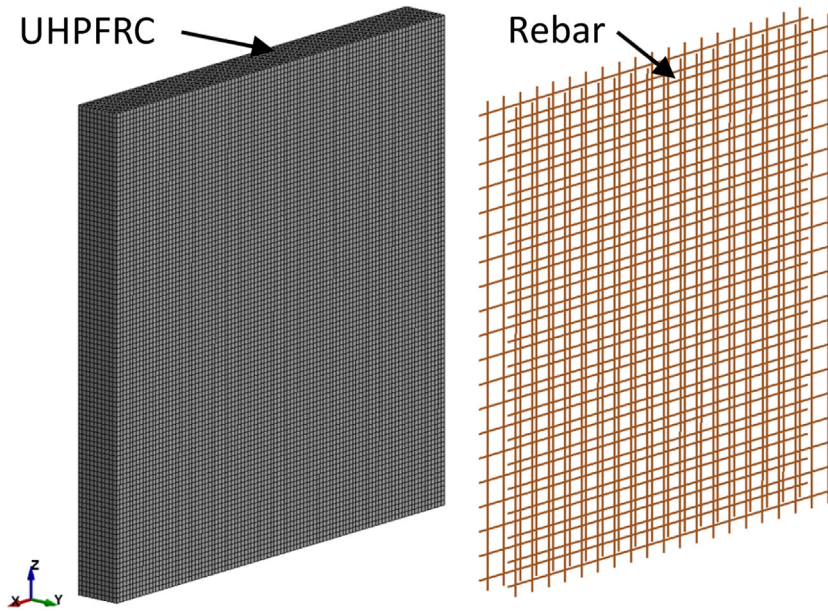


Fig. 2. FE model of the panel.

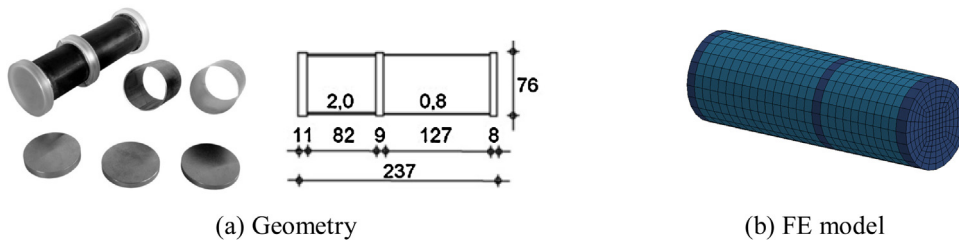


Fig. 3. Aircraft engine model [1].

Table 1
Material Properties.

Material	Exp. No.	Modulus of elastic E (GPa)	Poisson Ratio ν	Density ρ (Kg/m ³)	UCS (MPa)	UTS (MPa)	Failure strain (%)	Aggregate size (m)
Concrete	1	56.242	0.20	2500	182.8	9.5	–	0.008
	2	55.577	0.20	2500	172.1	9.2	–	0.008
	3	55.085	0.20	2500	186.0	9.6	–	0.008
	4	54.922	0.20	2500	174.5	9.3	–	0.008
Rebar steel	All	200	0.3	7850	447.2	447.2	25	–
Missile steel	All	210	0.3	7850	355.0	355.0	–	–

Table 2
Total element numbers of the FE model.

Components	Beam elements	Shell elements	Solid elements
Wall	–	–	100,000
Rebar	3200	–	–
Missile	–	600	468
Total	3200	600	100,468

was defined as the slave part, whereas the segment set of concrete panel was defined as the master part. The option *AUTOMATIC_NODES_TO_SURFACE was used for the aircraft engine model-rebar contact. The node set of the rebar was defined as the slave part, while the segment set of the aircraft engine model was defined as the master part. The fixed supported boundary conditions were applied to the reference nodes of the panel.

Initial velocities were applied to the aircraft engine node set using the option *INITIAL_VELOCITY. In order to reduce the analysis time, the initial location of the front head of the aircraft engine model was set directly on the face of the panel. An

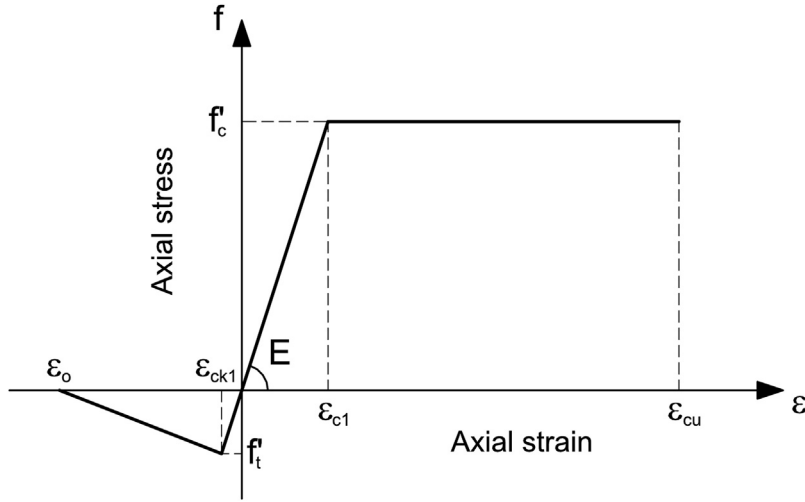


Fig. 4. Bi-linear concrete model.

analysis time of 20 ms was allotted in order to observe complete perforation. The time interval between outputs of 1E–4 s was applied to obtain a continuous behavior. Hourglass control with the stiffness form of Flanagan-Belytschko integration ($IHQ=4$) was selected. In LS-DYNA, the contact between the slave and master parts was taken into account using coupling interaction analysis.

2.2. Material models

The material models used in this study, including concrete and steel were presented by Thai and Kim [10]. Nevertheless, they are briefly presented here for the reader's convenience.

2.2.1. Concrete

Although there are several concrete models provided by LS-DYNA such as Concrete_Damage (MAT#072), Winfrith_Concrete (MAT#084), CSCM_Concrete (MAT#159)... , it is found that the Winfrith model was the best choice for modeling the punching behavior of UHPFRC panel under impact loading. Therefore the Winfrith material model (MAT#084), considering the strain-rate in LS-DYNA [11], was used for the concrete panel. Fig. 4 shows the bi-linear concrete model using an equivalent uniaxial stress-strain curve. The elastic-plastic curve with the ultimate strain (ϵ_{cu}) at the failure assumed for the concrete compressive model. The assumed concrete tension model was the linear tension softening behavior with the axial strain (ϵ_{ck1}) at the failure. The tensile fracture strain (ϵ_o) was determined as a function of the fracture energy of the concrete.

The Winfrith concrete model does not consider erosion for damage and failure. In this study, the erosion option was activated by using additional keyword *MAT_ADD_EROSION (M#000). The suitable value for the erosion option was defined using sensitivity analysis as presented in Section 4.

The strain-rate effect was automatically considered in the Winfrith concrete model. Fig. 5 shows the stress-strain curves with respect to various strain rates. The concrete strengths were calculated by multiplying the original values with the strain-rate enhancement factors. The tensile (E_T) and compressive (E_C) factors were calculated using the equations below [11].

Calculation is made with a low strain-rate when $\dot{\epsilon} < 30s^{-1}$:

$$E_T = \left(\frac{\dot{\epsilon}}{\dot{\epsilon}_{0T}} \right)^{1.016\delta} \quad \text{and} \quad E_C = \left(\frac{\dot{\epsilon}}{\dot{\epsilon}_{0C}} \right)^{1.026\alpha}, \quad (1)$$

and high strain-rate when $\dot{\epsilon} > 30s^{-1}$:

$$E_T = \eta \dot{\epsilon}^{1/3} \quad \text{and} \quad E_C = \gamma \dot{\epsilon}^{1/3}, \quad (2)$$

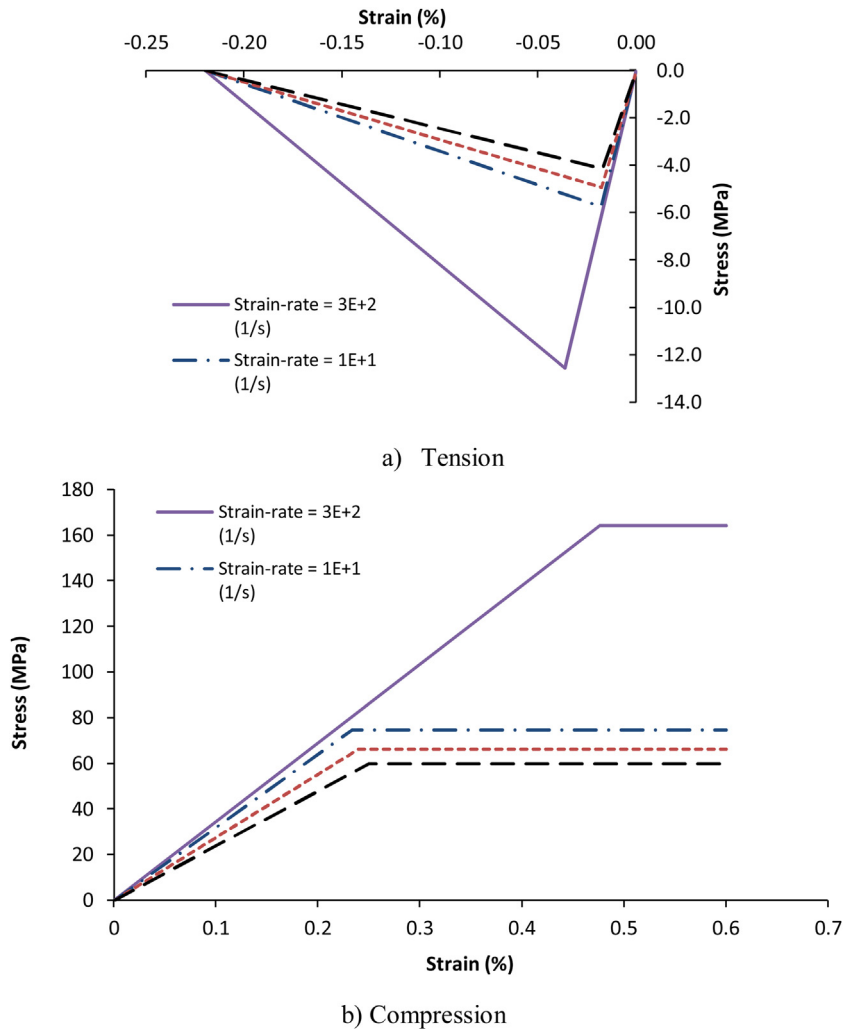


Fig. 5. Stress-strain curve of concrete with various strain-rates.

Table 3

Calculated strain-rate factors corresponding to $f_{cu} = 72.5$ MPa.

Factor type	0	0.01/s	10/s	300/s
E_T	1.00	1.20	1.39	3.05
E_C	1.00	1.11	1.25	2.74
E_E	1.00	1.15	1.33	1.43

where: $\delta = \frac{1}{10+0.5f_{cu}}$; $\alpha = \frac{1}{5+0.75f_{cu}}$; $\log_{10}\eta = 6.933\delta - 0.492$; $\log_{10}\gamma = 6.156\alpha - 0.492$; $\dot{\epsilon}_{0T} = 3 \times 10^{-6}s^{-1}$; and $\dot{\epsilon}_{0C} = 30 \times 10^{-6}s^{-1}$. here, f_{cu} is the concrete cube strength (unit in MPa). Young's modulus rate enhancement was calculated using the following equation:

$$E_E = 0.5 \left[\left(\frac{\dot{\epsilon}}{\dot{\epsilon}_{0T}} \right)^{0.016} + \left(\frac{\dot{\epsilon}}{\dot{\epsilon}_{0C}} \right)^{0.026} \right]. \quad (3)$$

Table 3 presents calculated tensile, compressive, and modulus factors with respect to various strain rates corresponding to concrete compressive strength $f_{cu} = 72.5$ MPa.

2.2.2. Steel rebar

Fig. 6 shows the elastic plastic with the kinematic hardening material model (MAT#003) in LS-DYNA, which was used to model the behavior of the steel rebar [12]. In this study, kinematic hardening was considered by setting parameter $\beta = 0$.

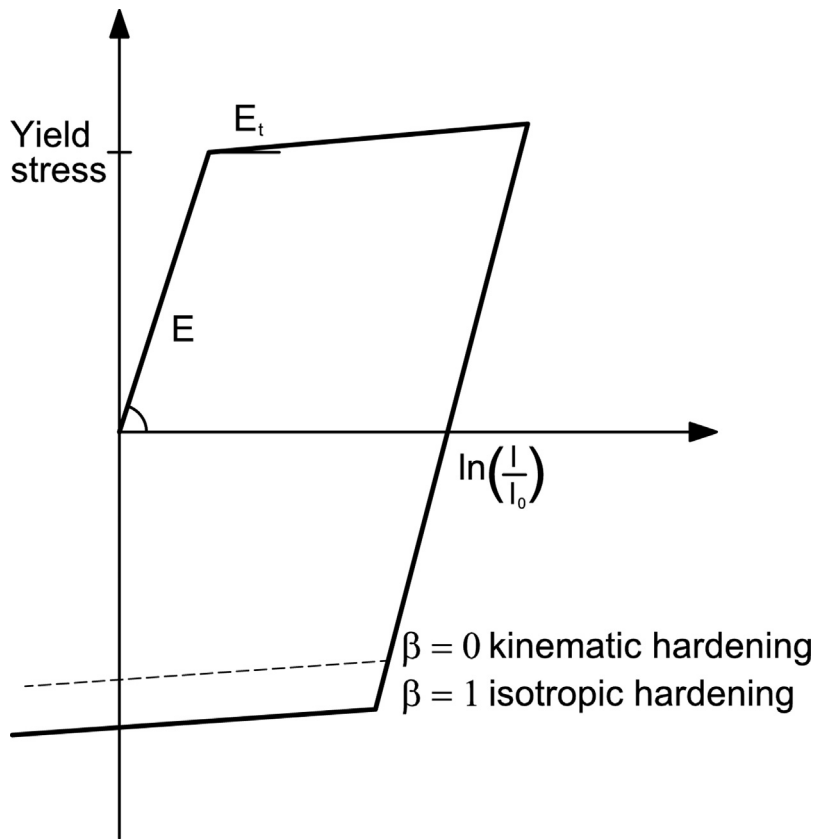


Fig. 6. Elastic-plastic behaviors with kinematic/isotropic hardening.

The yield strength of the steel was highly strain-rate dependent. This dynamic yield strength of the steel was taken into consideration by the Cowper-Symonds formula for uniaxial tension or compression [13]:

$$\frac{\sigma_d}{\sigma_s} = 1 + \left(\frac{\dot{\epsilon}}{C} \right)^{\frac{1}{P}}, \quad (4)$$

where σ_d is the dynamic yield strength, σ_s is the static yield strength, $\dot{\epsilon}$ is the strain-rate, and C and P are the constants of the Cowper-Symonds relation. For the rebar and structural steel, the constants $C = 40.4 \text{ s}^{-1}$ and $P = 5$ proposed by Jones [14] were used. Fig. 7 shows the stress-strain curves with respect to the various strain-rates of the steel.

2.2.3. Steel aircraft

A piecewise linear isotropic plasticity material model (MAT#024) was used to model the behavior of the steel used on the aircraft engine model. In this study, the hardening behavior of the material model was not considered, as shown in Fig. 8 (i.e. ETAN=0). The strain-rate effects are beyond the scope of this study.

3. Verification of numerical analysis

The analysis results were verified by comparing them with the experimental results conducted by Riedel et al. [1]. For the purposes of the verification, a sensitivity study with different erosion values was performed. The material erosion for damage and failure was considered by using the option *MAT_ADD_EROSION. This option has a total of 14 different erosion criteria. According to sensitivity studies conducted by Sagals et al. [15] and the works of Thai and Kim [16], the principal strain was shown to be the most sensitive erosion criterion. The principal strains from $\pm 7\%$ to $\pm 11\%$ were used for the parametric analysis. Fig. 9 shows the relationship between the residual velocity and principal strain. Fig. 10 shows the relationship between the scabbing area and principal strain. It can be seen that the analysis result of the residual velocity matched that of the test when the principal strain was $\pm 9.8\%$, whereas the analysis result of the scabbing area matched that of the test when the principal strain was $\pm 9.4\%$. As a result, the principal strain of $\pm 9.6\%$ was defined as the most suitable EROSION.

Four experiments by Riedel et al. [1] (Exp. No.1–4) were used for the verification. Good agreement of the damage of the panels between the experiments and numerical analyses was achieved as shown in Fig. 11 and Table 4. The deformation of the aircraft engine model of the FE modeling also agreed well with the test results as shown in Fig. 12. These results showed

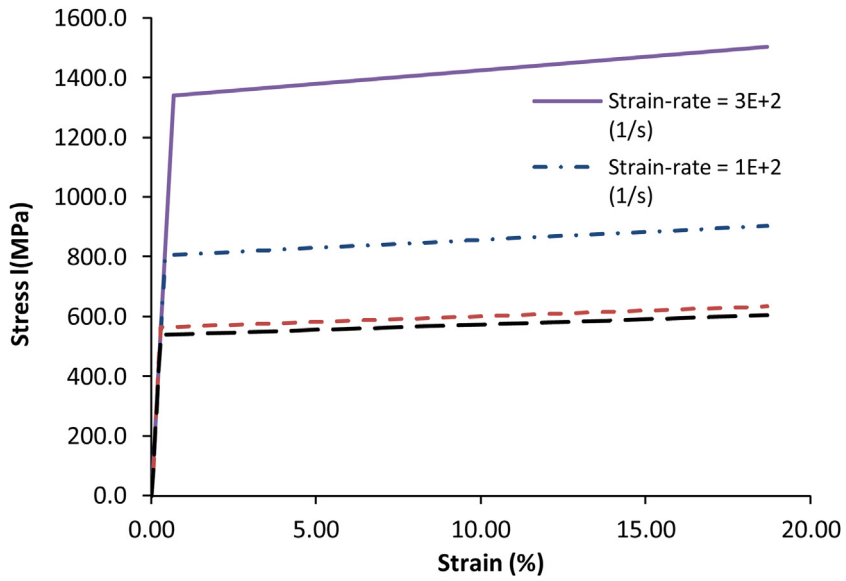


Fig. 7. Stress-strain curve of steel with various strain-rates.

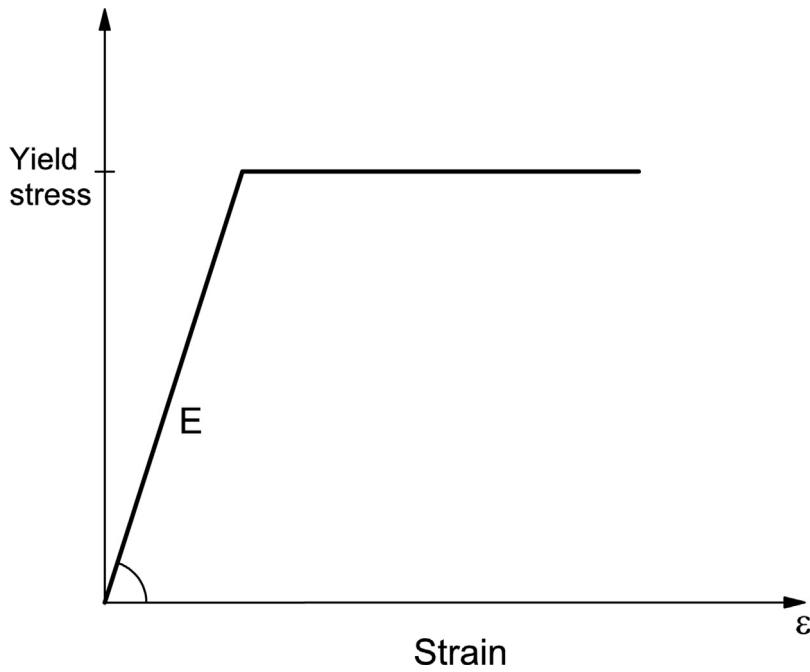


Fig. 8. Steel material model considering elastic-plastic behaviors.

that the developed finite element model reliably predicted the failure mode and damage of the UHPFRC panel under aircraft engine model impact.

4. Parametric study

This section presents a parametric analysis of the UHPFRC panels under engine model impact to study the degree of local damage to the panel with respect to different parameters. Table 5 lists the most influential variables as the analysis parameters.

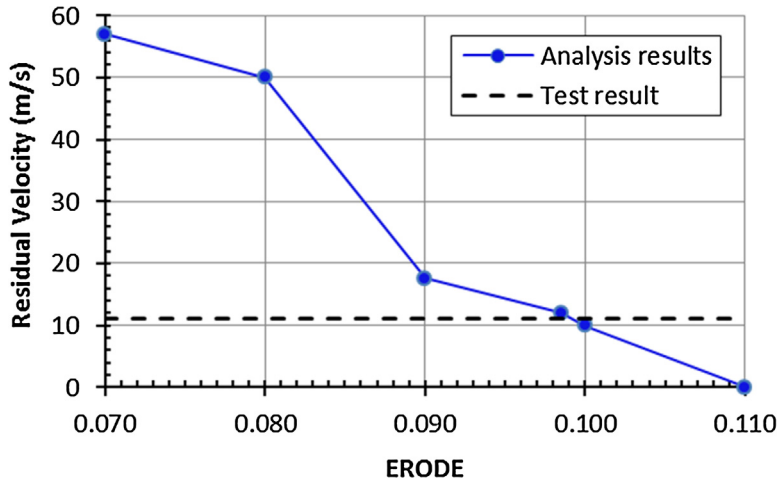


Fig. 9. Relationship between ERODE and residual velocity.

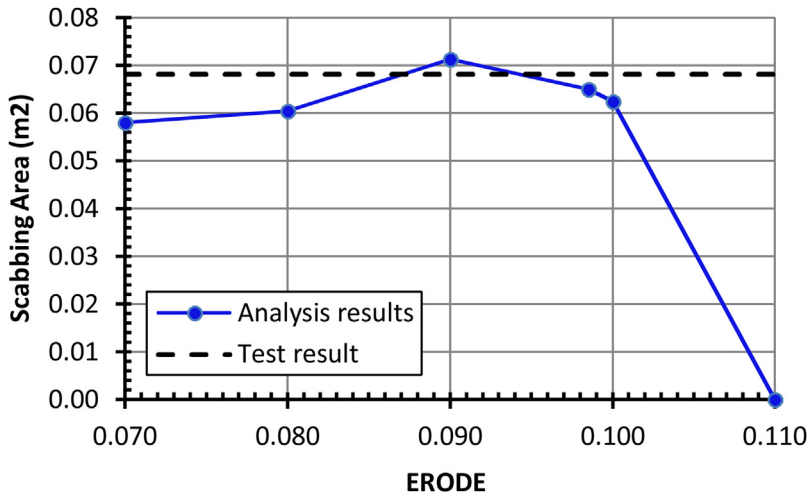


Fig. 10. Relationship between ERODE and scabbing area.

Table 4
Comparison of the analysis results with those of the experiments.

Exp. No.	Method	Initial velocity (m/s)	Panel failure mode ^a	Residual velocity (m/s)	Scabbing Area (m ²)	Deflection (mm)	Missile failure mode
1	Exp.	194.7	C	-0.86	-	2.00	Bucked
	FEM	194.7	C	-0.82	-	2.21	Bucked
	Difference	0	-	4.7%	-	10.5%	-
2	Exp.	258.7	JS	-0.73	-	12.00	Bucked
	FEM	258.7	JS	-0.69	-	13.12	Bucked
	Difference	0	-	5.5%	-	9.33%	-
3	Exp.	320.0	JP	0.00	0.0837	-	Crushed
	FEM	320.0	JP	0.00	0.0789	-	Crushed
	Difference	0	-	0.0%	5.7%	-	-
4	Exp.	332.0	P	11.00	0.0775	-	Crushed
	FEM	332.0	P	12.00	0.0650	-	Crushed
	Difference	0	-	9.10%	16.1%	-	-

^a C = Penetration Mode, JS = Just Scabbing Mode, JP = Just Perforation Mode, P = Perforation Mode.

The parameters of fiber type and content were varied using the corresponding tensile strength of UHPFRC. The tensile strength of the FRC composite can be calculated using the model proposed by Naaman [17]. The first and the post cracking strengths (see Fig. 13) can be calculated using the following equations suggested by Naanman [17]:

$$\sigma_{cc} = \sigma_{mu}(1 - V_f) + \alpha \tau_{eq} V_f \frac{l_f}{\phi_f} \tag{5}$$

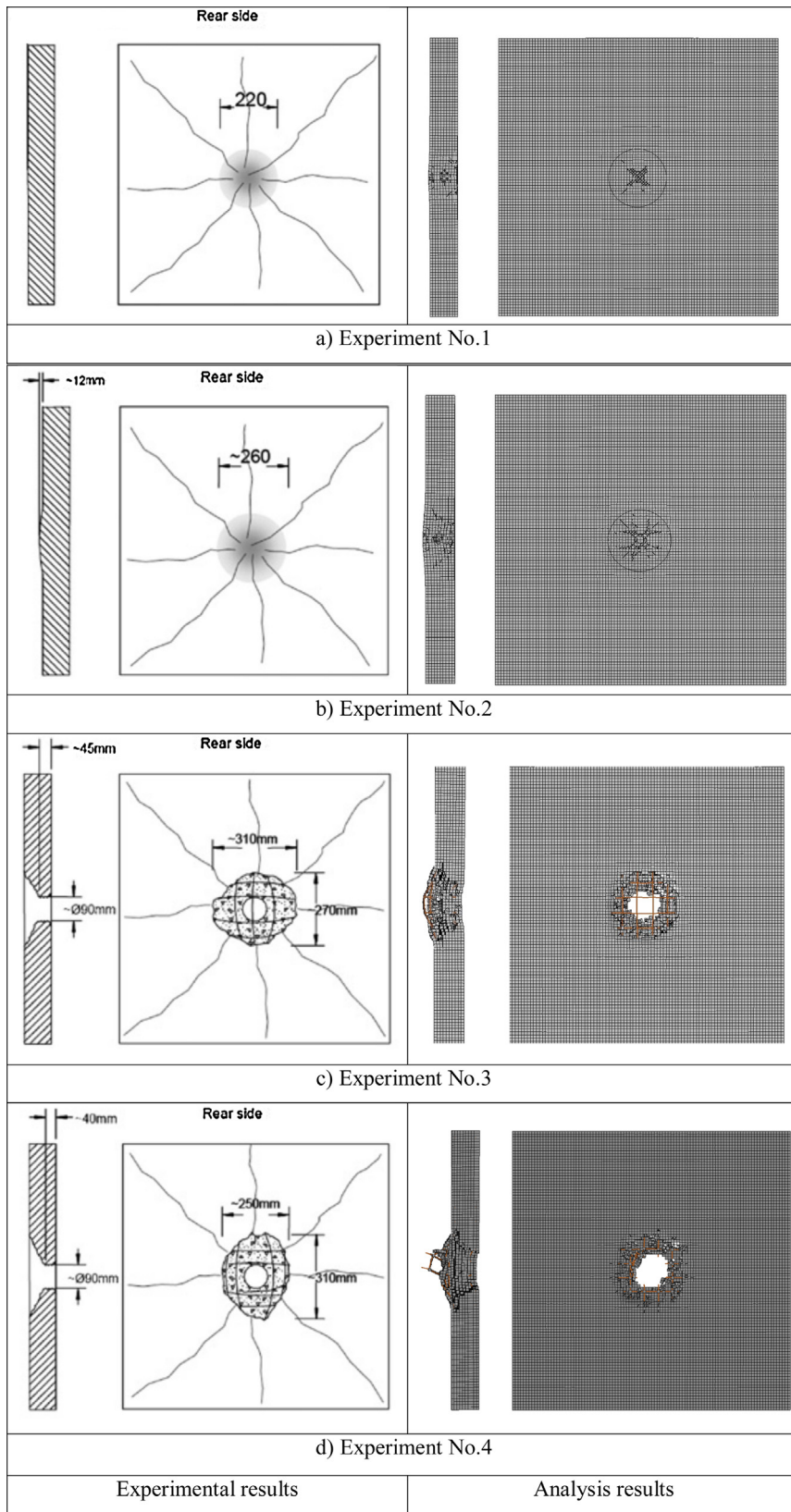


Fig. 11. Comparison of damage of the panel.

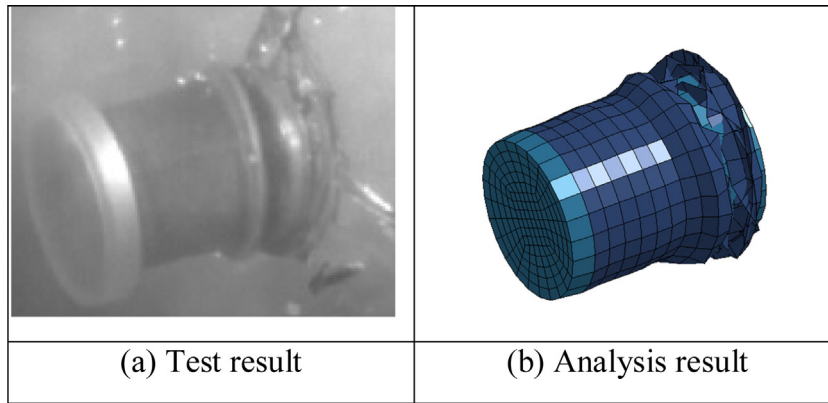


Fig. 12. Comparison of missile deformation (Exp. No. 1).

Table 5
Selected parameters.

Variable	Range of variable
Missile velocity (m/s)	100, 150, 200, and 250
Fiber type	Hooked and Torex
Fiber content (%)	1.0 and 2.0
Panel thickness (m)	0.03–0.12

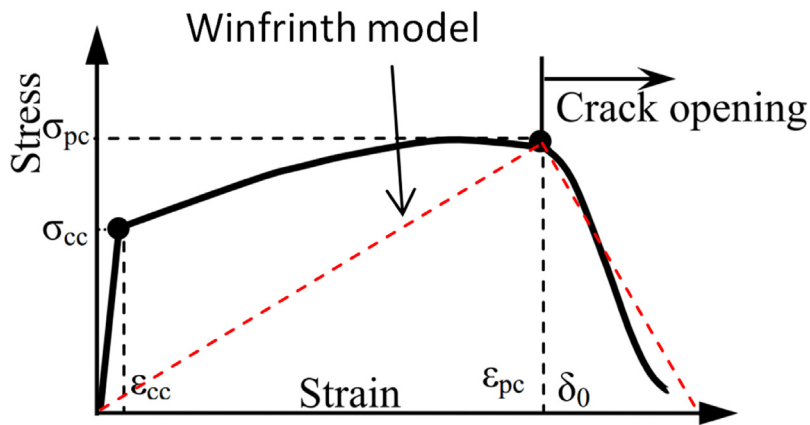


Fig. 13. Typical stress-strain curve of FRC.

Table 6
Properties of fibers used in this study.

Fiber type	Diameter (mm)	Length (mm)	Bond stress (MPa)
Hooked	0.4	30	4.73
Torex	0.3	30	14.49

for the first cracking strength, and

$$\sigma_{pc} = \lambda_{pc} \tau_{eq} V_f \frac{l_f}{\phi_f} \tag{6}$$

for the post cracking strength, where V_f is the fiber content by volume, l_f is the fiber length, ϕ_f is the fiber diameter, σ_{mu} is the tensile strength of matrix, τ_{eq} is the equivalent bond strength, α and λ_{pc} are the coefficients.

This analysis used Hooked and Torex fiber for the UHPFRC panels. The panels had rebars with a diameter of 5.5 mm and a spacing of 50 mm in both faces and directions. The Hooked and Torex fiber used in this study were adopted from the works of Kim [18]. Certain properties of the fibers are shown in Table 6. The behaviors of panels were investigated considering different fiber content of 1.0% and 2.0%. The compressive strength of UHPFRC was assumed to be constant (150 MPa), whereas the maximum tensile strength was assumed to be the post cracking strength of UHPFRC.

Table 7
Calculated tensile strength of UHPFRC using Naaman's equation.

Fiber contents	Hooked fiber		Torex fiber	
	λ_{pc}	σ_{pc} (MPa)	λ_{pc}	σ_{pc} (MPa)
1.00%	2.03	7.19	0.71	10.22
2.00%	1.47	10.45	0.44	12.73

Table 8
Input parameters and corresponding analysis results (1.0% Hooked fiber).

Specimen No.	Panel thickness (m)	Impact velocity (m/s)	Failure mode ^a
S1.1	0.03	100	S
S1.2	0.04	100	JS
S1.3	0.05	100	C
S1.4	0.06	100	C
S1.5	0.03	150	P
S1.6	0.04	150	JP
S1.7	0.05	150	S
S1.8	0.06	150	JS
S1.9	0.08	150	C
S1.10	0.04	200	P
S1.11	0.05	200	JP
S1.12	0.06	200	S
S1.13	0.08	200	C
S1.14	0.10	200	C
S1.15	0.05	250	P
S1.16	0.06	250	JP
S1.17	0.08	250	S
S1.18	0.10	250	C
S1.19	0.12	250	C

^a C = Penetration Mode, S = Scabbing Mode, JS = Just Scabbing Mode, JP = Just Perforation Mode, P = Perforation Mode.

Table 9
Input parameters and corresponding analysis results (2.0% Hooked fiber).

Specimen No.	Panel thickness (m)	Impact velocity (m/s)	Failure mode ^a
S2.1	0.03	100	S
S2.2	0.04	100	JS
S2.3	0.05	100	C
S2.4	0.06	100	C
S2.5	0.03	150	P
S2.6	0.04	150	S
S2.7	0.05	150	S
S2.8	0.06	150	C
S2.9	0.08	150	C
S2.10	0.04	200	P
S2.11	0.05	200	JP
S2.12	0.06	200	S
S2.13	0.08	200	C
S2.14	0.10	200	C
S2.15	0.05	250	P
S2.16	0.06	250	JP
S2.17	0.08	250	JS
S2.18	0.10	250	C
S2.19	0.12	250	C

^a C = Penetration Mode, S = Scabbing Mode, JS = Just Scabbing Mode, JP = Just Perforation Mode, P = Perforation Mode.

To calculate the post cracking strength, the coefficient λ_{pc} in equation (6) can be determined using the following equations suggested by Suwannakarn [19]:

$$\text{Hooked fiber : } \lambda_{pc} = -55.6 V_f + 2.58. \quad (7)$$

$$\text{Torex fiber : } \lambda_{pc} = -26.6 V_f + 0.97. \quad (8)$$

Table 7 shows the values of λ_{pc} and the corresponding tensile strengths of the UHPFRC for Hooked and Torex fiber as the function of fiber content.

The impact velocities of 100 m/s, 150 m/s, 200 m/s, and 250 m/s and different panel thickness from 0.03 m to 0.15 m were also treated as parameters in order to evaluate the vulnerability of the different panels. The input parameters and corresponding analysis results are shown in Table 8. The observed damage of the panel was classified into five modes,

Table 10
Input parameters and corresponding analysis results (1.0% Torex fiber).

Specimen No.	Panel thickness (m)	Impact velocity (m/s)	Failure mode ^a
S3.1	0.03	100	S
S3.2	0.04	100	JS
S3.3	0.05	100	C
S3.4	0.06	100	C
S3.5	0.03	150	P
S3.6	0.04	150	JP
S3.7	0.05	150	S
S3.8	0.06	150	C
S3.9	0.08	150	C
S3.10	0.04	200	P
S3.11	0.05	200	JP
S3.12	0.06	200	S
S3.13	0.08	200	C
S3.14	0.10	200	C
S3.15	0.05	250	P
S3.16	0.06	250	JP
S3.17	0.08	250	JS
S3.18	0.10	250	C
S3.19	0.12	250	C

^a C = Penetration Mode, S = Scabbing Mode, JS = Just Scabbing Mode, JP = Just Perforation Mode, P = Perforation Mode.

Table 11
Input parameters and corresponding analysis results (2.0% Torex fiber).

Specimen No.	Panel thickness (m)	Impact velocity (m/s)	Failure mode ^a
S4.1	0.03	100	S
S4.2	0.04	100	C
S4.3	0.05	100	C
S4.4	0.06	100	C
S4.5	0.03	150	P
S4.6	0.04	150	S
S4.7	0.05	150	JS
S4.8	0.06	150	C
S4.9	0.08	150	C
S4.10	0.04	200	P
S4.11	0.05	200	S
S4.12	0.06	200	JS
S4.13	0.08	200	C
S4.14	0.10	200	C
S4.15	0.05	250	JP
S4.16	0.06	250	S
S4.17	0.08	250	C
S4.18	0.10	250	C
S4.19	0.12	250	C

^a C = Penetration Mode, S = Scabbing Mode, JS = Just Scabbing Mode, JP = Just Perforation Mode, P = Perforation Mode.

following Sugano et al. [20], includes (1) *Perforation Mode* (marked with a symbol 'P'), (2) *Just Perforation Mode* (marked with a symbol 'JP'), (3) *Scabbing Mode* (marked with a symbol 'S'), (4) *Just Scabbing Mode* (marked with a symbol 'JS'), and *Penetration Mode* (marked with a symbol 'C'). Fig. 14 shows five different failure modes captured from analysis results.

5. Modified formulas used to predict the local damage

To predict the scabbing and perforation thickness of the RC wall under aircraft engine impact, NEI 07-13 [8] provided the formulas, adopted from the modified formulas of Chang and Degen, as follows:

-Wall thickness required to prevent scabbing

$$t_s = \alpha_s 1.84(200/V)^{0.13}(MV^2)^{0.4}/(\{D/12\}^{0.2}\{144f'_c\}^{0.4}), \quad (9)$$

-Wall thickness required to prevent perforation

$$t_p = \alpha_p D \{2.2(x_c/\{\alpha_c D\}) - 0.3(x_c/\{\alpha_c D\})^2\}, \text{ for } x_e/\{\alpha_c D\} \leq 1.52. \quad (10)$$

where V is the engine velocity (ft/sec), $M = W/g$ where $g = 32.2$ (ft/sec²) and W is the total engine weight (lbs), D is the average outer diameter of the engine casing (inches), x_c is penetration depth, f'_c is the concrete strength (psi), α_c , α_s , and α_p are reduction factors for penetration depth, scabbing, and perforation thickness, respectively. The recommended values for α_c is 0.5, for α_s is 0.55, and for α_p is 0.6 based on the test results of Sugano et al. [7].


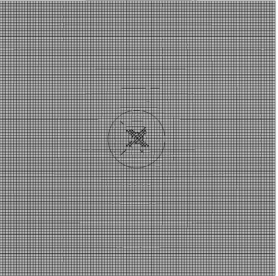

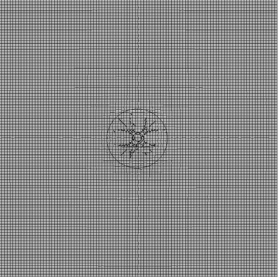

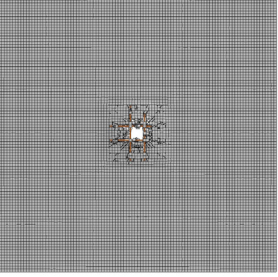

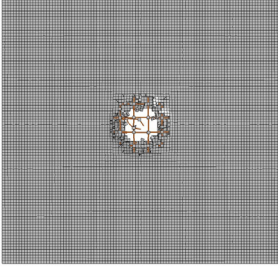

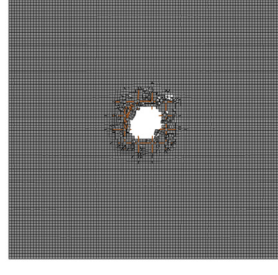
Failure modes	Image of failures	
Penetration		
Just scabbing		
Scabbing		
Just perforation		
Perforation		

Fig. 14. Failure modes of the panel.

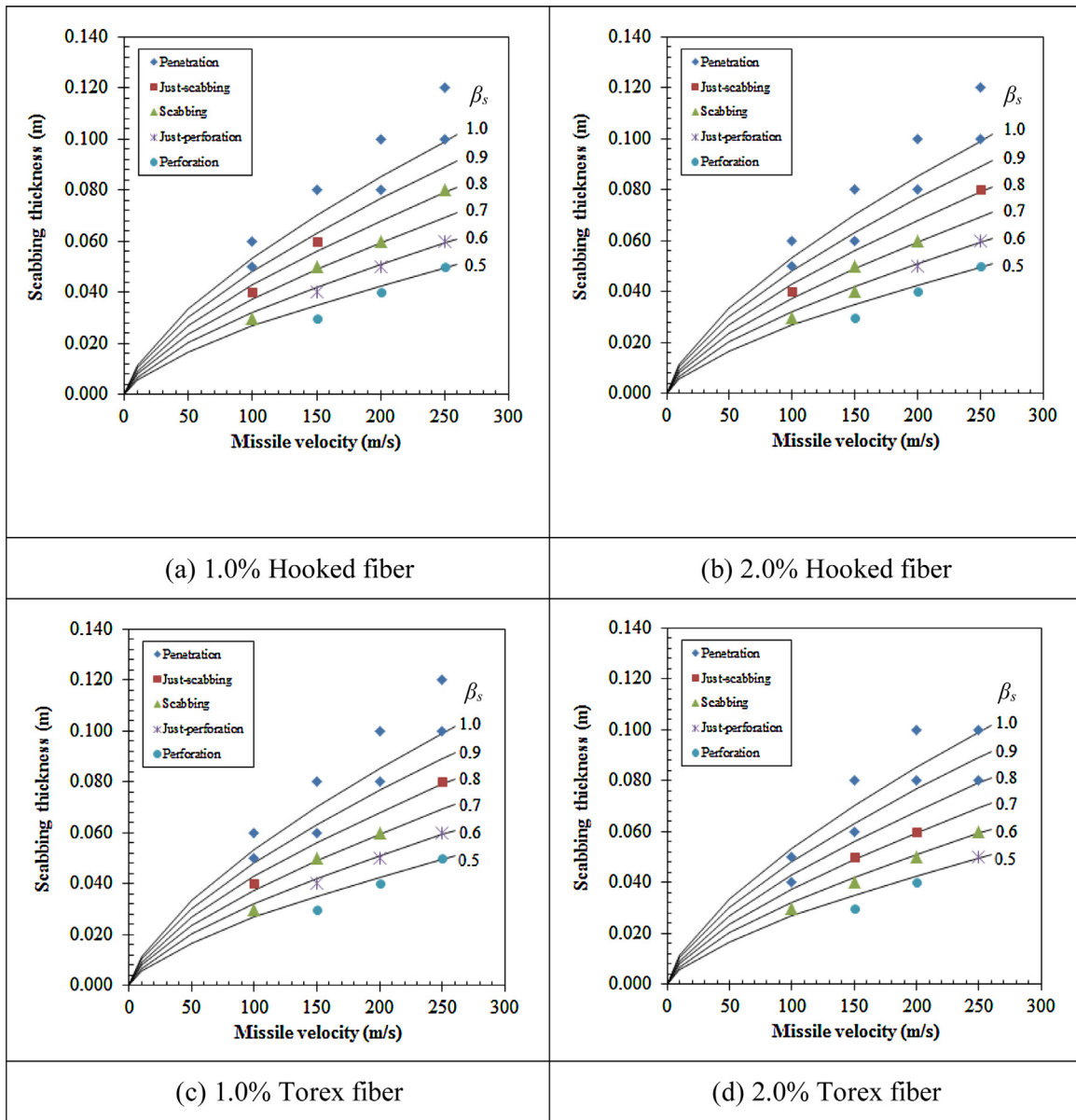


Fig. 15. Scabbing thickness.

A higher punching resistance capacity of the UHPFRC panel is expected to reduce local damage compared with that of the RC panel. For quantitation of the reduction in local damage, the following factors were newly introduced into this study:

- (1) Reduction factor for scabbing (β_s): The ratio of minimum panel thickness required to prevent scabbing damage mode of the UHPFRC panel to that required to prevent scabbing damage mode of the RC panel.
- (2) Reduction factor for perforation (β_p): The ratio of minimum panel thickness required to prevent perforation damage mode of the UHPFRC panel to that required to prevent perforation damage mode of the RC panel.

These reduction factors were evaluated from a comparison of panel thickness predicted by the empirical formulas (9) and (10) for the RC panels to the analysis results of the UHPFRC panels. The effect of fiber type and content on the reduction factors was included in this study (Table 9 Table 10 Table 11).

Fig. 15 shows a comparison of panel thickness required to prevent the scabbing damage mode predicted using equation (9) with various reduction factors for scabbing (β_s) to the analysis results of UHPFRC panels. It can be observed that for the panel with 1.0% Hooked fiber, the reduction factor can be defined as 0.85, as shown in Fig. 15a. For the panel with 2.0% Hooked fiber, the reduction factor can be defined as 0.82, as shown in Fig. 15b. For the panel with 1.0% Torex

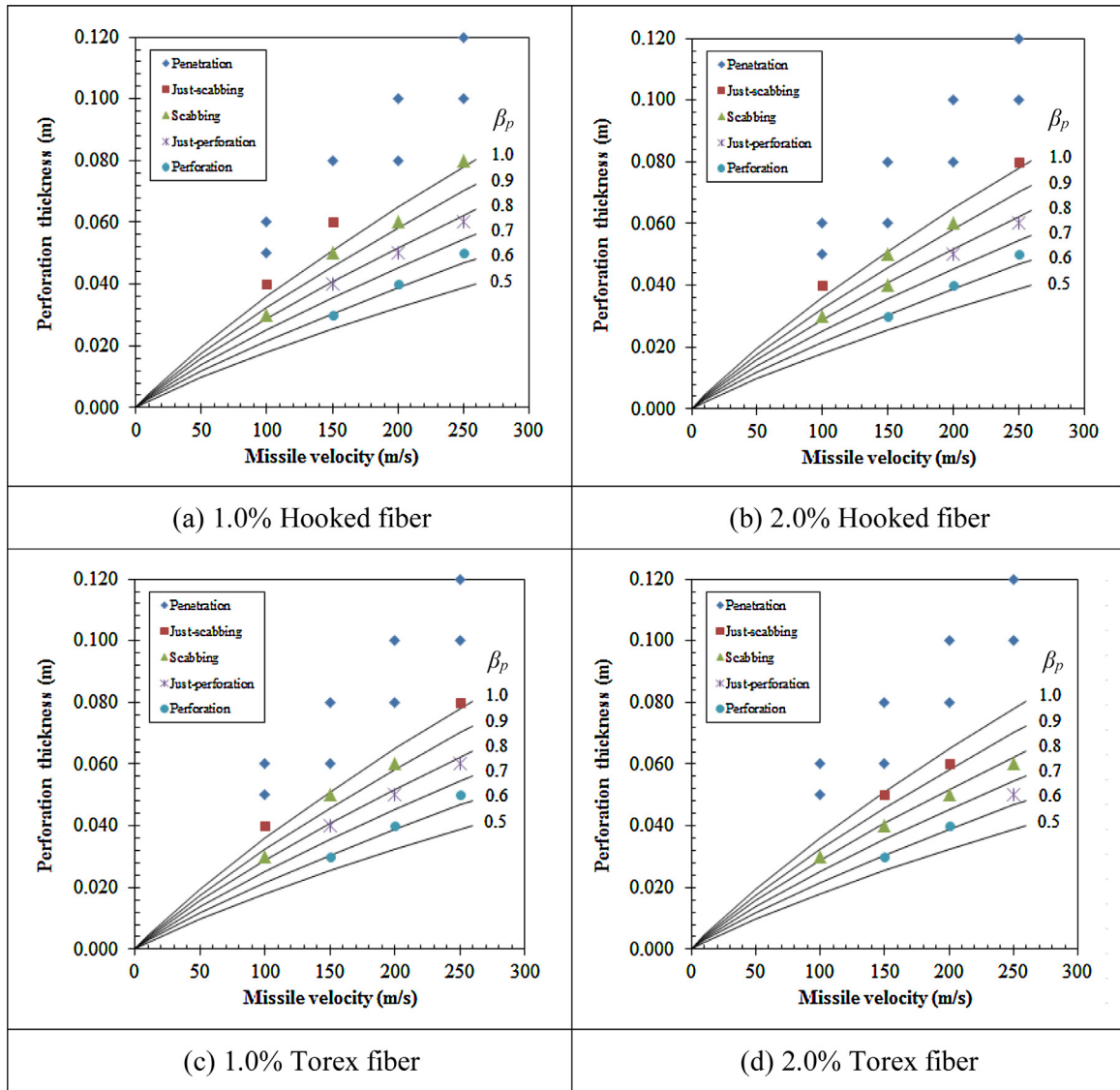


Fig. 16. Perforation thickness.

fiber 1.0% Torex fiber, the reduction factor can be defined as 0.82, as shown in Fig. 15c. For the panel with 2.0% Torex fiber, the reduction factor can be defined as 0.75, as shown in Fig. 15d.

Fig. 16 shows a comparison of panel thickness required to prevent perforation damage mode predicted using equation (10) with various reduction factors for perforation (β_p) to the analysis results of UHPFRC panels. It can be observed that for the panel with 1.0% Hooked fiber, the reduction factor can be defined as 0.80, as shown in Fig. 16a. For the panel with 2.0% Hooked fiber, the reduction factor can be defined as 0.77, as shown in Fig. 16b. For the panel with 1.0% Torex fiber, the reduction factor can be defined as 0.80, as shown in Fig. 16c. For the panel with 2.0% Torex fiber, the reduction factor can be defined as 0.70, as shown in Fig. 16d.

6. Conclusions

This paper presents numerical analyses of the UHPFRC panel under aircraft engine model impact. The structural components and their contacts were fully modeled. The impact test results were used to verify the finite element model, and the erosion option of concrete was considered in the analysis. The local damage to the UHPFRC panel was investigated with varying panel thicknesses, fiber types, and content as a parametric study. Different impact velocities were treated as parameters in order to evaluate the vulnerability of the different panels. The following conclusions were obtained:

- (1) The UHPFRC panels showed better capacity of punching resistance than that of the RC panels. In addition, fiber type and content had a significant effect on reducing the local damage of the panel.
- (2) In order to predict the scabbing and perforation thickness of UHPFRC panels subjected to an aircraft engine impact, the empirical formulas of Chang and Degen should be modified using the reduction factors. In the case in which the Hooked and Torex fiber, having ratio from 1.0% to 2.0% were used, the reduction factor for scabbing can be considered to be from 0.75 to 0.85 and the reduction factor for perforation can be considered to be from 0.70 to 0.80.

Acknowledgements

This work was supported by a grant from the Human Resources Development Program (No. 20124030200050) of the Korea Institute of Energy Technology Evaluation and Planning (KETEP), funded by the Ministry of Knowledge Economy of the Korean government.

References

- [1] W. Riedel, M. Nöldgen, E. Strabburger, K. Thoma, E. Fehling, Local damage to ultra high performance concrete structures caused by an impact of aircraft engine missiles, *Nucl. Eng. Des.* 240 (2010) 2633–2642.
- [2] R. Sovják, T. Vavriník, P. Máca, J. Zatloukal, P. Konvalinka, Y. Song, Experimental investigation of ultra-high performance fiber reinforced concrete slabs subjected to deformable projectile impact, *Procedia Eng.* 65 (2013) 120–125.
- [3] P. Máca, R. Sovják, P. Konvalinka, Mix design of UHPFRC and its response to projectile impact, *Int. J. Impact Eng.* 63 (2014) 158–163.
- [4] H. Adeli, A.M. Amin, Local effects of impactors on concrete structures, *Nucl. Eng. Des.* 88 (1985) 301–317.
- [5] J.D. Riera, Penetration, scabbing and perforation of concrete structures hit by solid missiles, *Nucl. Eng. Des.* 115 (1989) 121–131.
- [6] I. Kojima, An experimental study on local behavior of reinforced concrete slabs to missile impact, *Nucl. Eng. Des.* 130 (1991) 121–132.
- [7] T. Sugano, H. Tsubota, Y. Kasai, N. Koshika, C. Itoh, K. Shirai, W.A. Von Riesenmann, D.C. Bickel, M.B. Parks, Local damage to reinforced concrete structures caused by impact of aircraft engine missiles-Part 2. Evaluation of test results, *Nucl. Eng. Des.* 140 (1993) 407–423.
- [8] N.E.I. 07-13, Methodology for Performing Aircraft Impact Assessments for New Plant Designs (NEI 07-13 Revision 8P).2011, Nuclear Energy Institute, Washington, D.C. USA.
- [9] Livermore Software Technology Corporation, LS-DYNA Keyword User's Manual Version 971, 2007.
- [10] D.K. Thai, S.E. Kim, Numerical simulation of reinforced concrete slabs under missile impact, *Struct. Eng. Mech.* 53 (3) (2015) 455–479.
- [11] L. Schwer, *An Introduction to the Winfrith Concrete Model*, Schwer Engineering & Consulting Services, California, USA, 2010.
- [12] Livermore Software Technology Corporation, LS-DYNA Theory Manual, 2006.
- [13] S.T. Marais, R.B. Tait, T.J. Cloete, G.N. Nurick, Material test at high strain rate using the split Hopkinson pressure bar, *Latin Am. J. Sol. Struct.* 1 (2004) 319–339.
- [14] N. Jones, *Structural Impact*, Second edition, University Press, Cambridge, 2011.
- [15] G. Sagals, N. Orbovic, A. Blahoianu, Sensitivity studies of reinforced concrete slabs under impact loading, in: *Transactions of the 21st SMiRT*, New Delhi, India, November, 2011.
- [16] D.K. Thai, S.E. Kim, Failure analysis of reinforced concrete walls under impact loading using the finite element approach, *Eng. Fail. Anal.* 45 (2014) 252–277.
- [17] A.E. Naaman, *A Statistical Theory of Strength for Fiber Reinforced Concrete*, Massachusetts Institute of Technology, 1972.
- [18] D.J. Kim, Strain Rate Effect on High Performance Fiber Reinforced Cementitious Composites Using Slip Hardening High Strength Deformed Steel Fibers, The University of Michigan, 2009.
- [19] S.W. Suwannakarn, *Post-cracking Characteristics of High Performance Fiber Reinforced Cementitious Composites*, The University of Michigan, 2009.
- [20] T. Sugano, H. Tsubota, Y. Kasai, N. Koshika, H. Ohnuma, W.A. Von Riesenmann, D.C. Bickel, M.B. Parks, Local damage to reinforced concrete structures caused by impact of aircraft engine missiles-Part 1 Test program, method and results, *Nucl. Eng. Des.* 140 (1993) 387–405.